ORIGINAL ARTICLE

Improvements in Segmentation Using Scatter and Photopeak Window Data for Attenuation Correction in Myocardial SPECT

Takao Kanzaki, MS[1], Shu Kasama, MD[2], Yasuyuki Takahashi, PhD[3] and Hirotaka Shimada[1]

Received: April 14, 2016/Revised manuscript received: June 21, 2016/Accepted: June 28, 2016

Abstract

***Background*: The method of Segmentation with Scatter and Photopeak window data in Attenuation Correction (SSPAC) recognizes the outlines of the body around chest and lungs using scatter window data after which an attenuation correction (μ) map can be constructed. We have developed a new extraction method, adding a masking process to SSPAC, because the extraction of outlines was otherwise incomplete.**

***Methods and Results*: The masking process extracted right and left lung fields from chest images. The quality of the masking process was confirmed by the results from a low count phantom. In a case study, automatic extraction by SSPAC had a 44% success rate for low count (stress condition) myocardial single-photon emission computed tomography (SPECT) images, but reached a success rate of 99% with the addition of the new masking process. Outline truncation and low counts can cause unsuccessful SSPAC.**

***Conclusions*: Our method for masking will contribute to a widespread use of SSPAC by improving the success rate in contouring.**

Keywords: Masking process, SSPAC, Stress condition

Ann Nucl Cardiol 2016；2（1）：38-43

Scatter correction and attenuation correction, as well as resolution correction, are used to improve the quantification accuracy of single-photon emission computed tomography (SPECT) images of the myocardium. Attenuation correction requires a μ map, which is usually derived using an external source (1), or from a CT image (2). Problems associated with these common methods include a longer image acquisition time and increased radiation dose to the patient. Furthermore, with the SPECT/CT method of attenuation correction, accuracy is decreased by any misregistration of the CT and SPECT images (3).

The SSPAC method, which recognizes the outlines of the body around chest and lungs using scatter window data, is known to reduce misregistration problems by its method of constructing a μ map (4). However, when injecting a low dose, the quality of the Compton scatter image and the recognition accuracy of the outlining decrease (5), such that a μ map image cannot be constructed. Consequently, the SSPAC method has not been widely used. In this study, we developed a new method to improve the success rate of constructing a μ map with the SSPAC method, and tested it using phantom and clinical studies.

Materials and methods

Our modified SSPAC method constructs an attenuation coefficient map from projection data. First, the body outline and lung contours are segmented from the reconstructed Compton scatter image. The Compton scatter image is reconstructed from the projection counts acquired in the lower window adjacent to the main window of the triple energy window (TEW) scatter correction method (6). Second, the myocardium and the liver are segmented based on the image

doi：10.17996/ANC.16003

1) Takao Kanzaki, Hirotaka Shimada
Department of Radiology, Gunma University Hospital, 3-19-15 Showa, Maebashi, Gunma, Japan 371-8511
E-mail: tkanzaki@gunma-u.ac.jp
2) Shu Kasama
Department of Medicine and Biological Science (Cardiovascular Medicine), Gunma University Graduate School of Medicine, Maebashi, Japan
3) Yasuyuki Takahashi
Department of Nuclear Medicine Technology, Gunma Prefectural College of Health Sciences, Maebashi, Japan

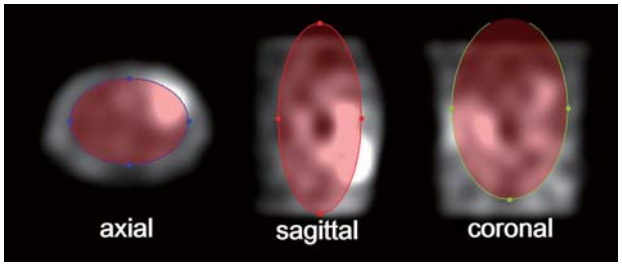

Fig. 1 Masking process is used to extract the left and right lung fields from the Compton scatter image. The edge of the mask is verified to be outline of the lung contour. The mask range is shown in red circle.

reconstructed from projection counts in the photopeak window. The outline extraction can fail when the patient has been administered only a low dose of ^{99m}Tc-tetrofosmin (TF) (4).

To improve this; third, filtering of the projection data is added to improve the SN ratio. Fourth, a new masking process is used to extract the left and right lung fields from the chest image. Fifth, the edge of the mask is verified to be in agreement with the longest outline of the lung contour. Sixth, the mask range is adapted for horizontal and vertical lung ranges. The body outlines, lung contours, myocardium, and the liver are extracted clearly by this mask processing (Fig. 1). Seventh, the body outline, lung contours, myocardium outline, and the liver outline are attached to images of the mediastinum and thoracic spine region, obtained by computed tomography. Eighth, an attenuation coefficient map is generated using attenuation values for bone, soft tissue, and lung of 0.30, 0.150, and 0.03 cm^{-1}, respectively. This image processing is semi-automatic (Fig. 2).

System parameters

An E-CAM (Toshiba Medical Systems, Otawara, Tochigi, Japan) dual-detector gamma camera system equipped with low-to-medium-energy general-purpose collimator was used. The matrix size was 64×64, and the reconstructed pixel size was 6.6×6.6 mm. The energy for ^{99m}Tc was set at 140±15.0 % keV. The scattered radiation estimate window was set to both sides of the photon peak window by the 7% window width.

Myocardial phantoms were scanned at 6-degree intervals over 360 degrees using continuous mode SPECT, with a pair of detectors repeatedly acquiring 180-degree data over 1 minute. The SPECT images were reconstructed using the data from each rotation. Based on a calculated rotation count, stress-condition images were acquired using three rotations, and resting-condition images were acquired using ten rotations. Patients were scanned with Quantitative Perfusion SPECT (QPS) at 6-degree intervals over 360 degrees (30 s/step, 20 min in total) in a supine position using step-and-shoot mode.

Attenuation correction maps were generated using a GMS-7700R workstation (Toshiba Medical Systems, Otawara, Tochigi, Japan). Reconstruction was based on implementation of the ordered subsets- expectation maximization (OS-EM) algorithm (7,8). A Butterworth filter (photopeak image: order 8, cutoff frequency=0.53 cycles/cm; Compton scatter image: order 8, cutoff frequency=0.21 cycles/cm) was used as a pre-filter. The TEW method was used for scatter correction (6).

Phantom study

The phantom study was performed using two kinds of myocardial phantom; the Heart-Liver Phantom (Model HL, Kyoto Kagaku Co., Ltd, Kyoto, Japan) and the Anthropomorphic Torso Phantom™ (Model ECT/TOPR/P, Data Spectrum Co., Hillsborough, NC, USA). A tracer (^{99m}Tc) with a radioactivity concentration of 74.0 kBq/ml was infused into the region of the myocardium. A concentration of 25.0kBq/ml was infused into the lung and the liver, and 15.0kBq/ml was infused into the mediastinum. The comparisons in this phantom study were between: 1) a lower count (stress condition) study without SSPAC (NONE), 2) a lower count (stress condition) study using SSPAC automatic processing without the masking process (AUTO), 3) a lower count (stress condition) study using SSPAC automatic processing with the masking process (MASK), and 4) a higher count (resting condition) study with SSPAC automatic processing (REST). The stress-condition study employed three rotations, while the resting-condition study employed ten rotations.

Case study

The accuracy of the mask processing of SSPAC was compared in the right coronary artery (RCA), left anterior descending coronary artery (LAD) or left circumflex coronary artery (LCX) regions using the contrast ratio of the normal group in which automatic processing was successful. Comparisons of the contrast ratios before and after SSPAC were made for the NONE, AUTO and MASK groups in the stress condition. Thirty normal subjects (20 men and 10 women; mean age 70.7±11.1 years; range 43-89 years) underwent myocardial SPECT. For the stress or resting conditions, 300 MBq or 900 MBq of ^{99m}Tc-tetrofosmin, respectively, was injected intravenously; data acquisition was initiated 30 min after the injection. This case study was approved by the Ethics Committee of Gunma University (No. 15-102).

Statistical analysis

Normalized SPECT values (maximum standardized as 100%) were recorded as means±standard deviations (SD). Data were analyzed with SPSS software (version 23.0; SPSS

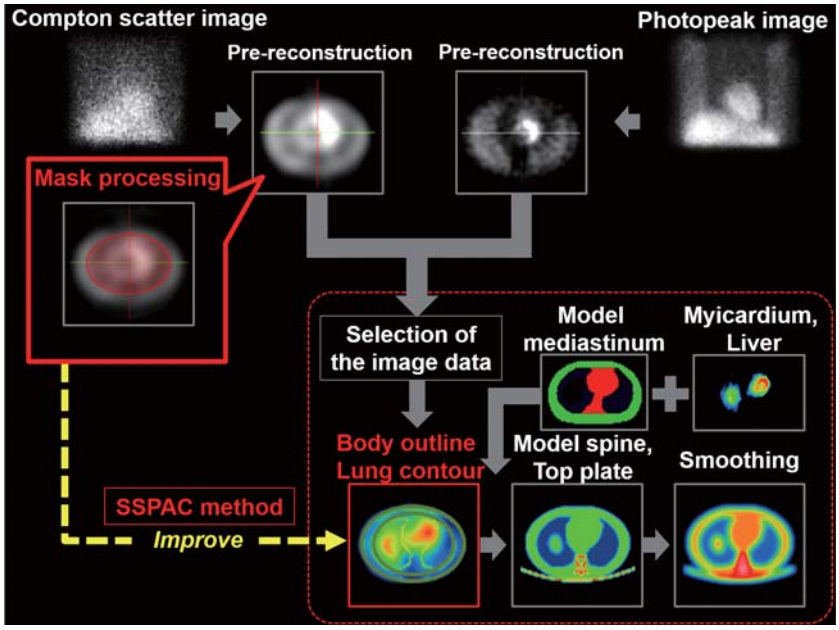

Fig. 2 The process for constructing segmentation with scatter and photopeak window data for attenuation correction (SSPAC), and a new masking process added to SSPAC.

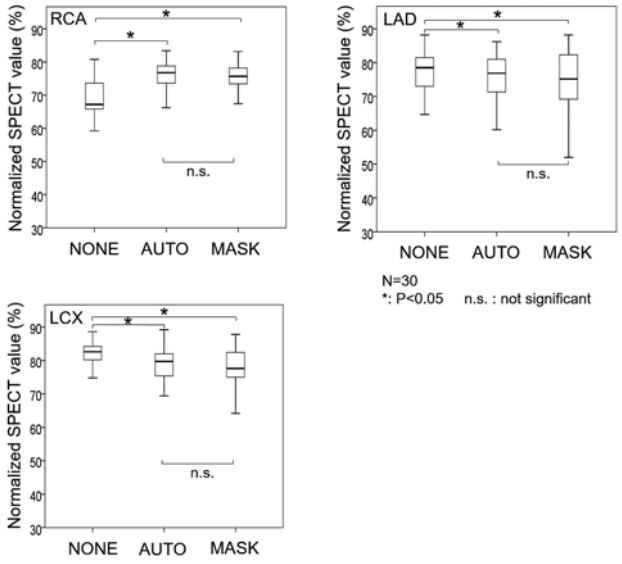

Fig. 3 Contrast ratios calculated using NONE, AUTO and MASK. Upper left: results with RCA area. Upper right: results with LAD area. Lower left: results with LCX area.

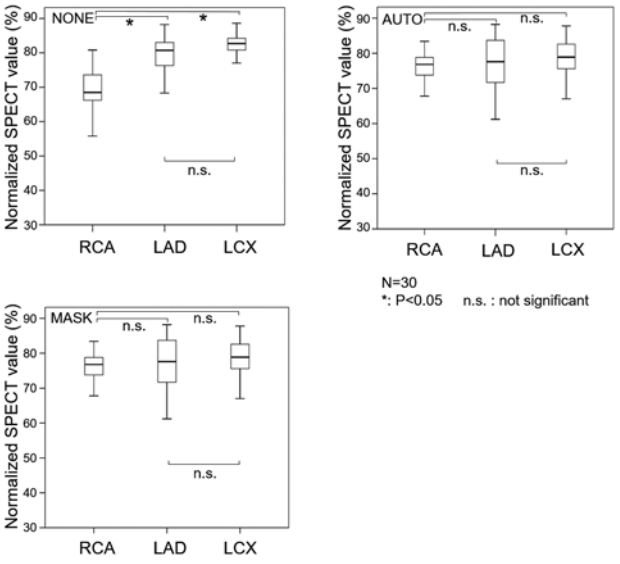

Fig. 4 Contrast ratios calculated using RCA, LAD and LCX. Upper left: results with NONE area. Upper right: results with AUTO area. Lower left: results with MASK area.

Inc.). One-way repeated-measures analysis of variance (SPSS), using by two-sided paired *t* test (Fig. 3) and Tukey's test (Fig. 4), was used to compare the three different image-processing routines of the SSPAC software. Probability values <0.05 were considered statistically significant.

Results

Fig. 5 shows SPECT images from the phantom studies. The type of phantom affected the count of the body outline and the trace success rate of the segmentation. Outline extraction failed with the low-count (3 rotations) images. However, the lung contour mask processing succeeded and a μ map could be made. All three correction approaches produced similar results. Seventeen divisions (The number of divisions is same as clinical Bull's eye map) of the normalized SPECT mean value (%) and SD (CV (%)) of Heart-Liver Phantom were 78.7 ± 8.1 (10.3) in NONE, 84.6 ± 6.9 (8.1) in AUTO, 84.2 ± 6.6 (7.9) in MASK, 83.9 ± 6.3 (7.6) in REST. Those values for the Anthropomorphic Torso Phantom™ were 80.8 ± 8.8 (10.9) in NONE, 83.7 ± 5.1 (6.2) in AUTO, 84.0 ± 5.2 (6.2) in MASK, 83.9 ± 4.2 (4.9) in REST.

In the normal study, the automatic success rate of SSPAC in the stress condition was 44%. The cause of failure was the low

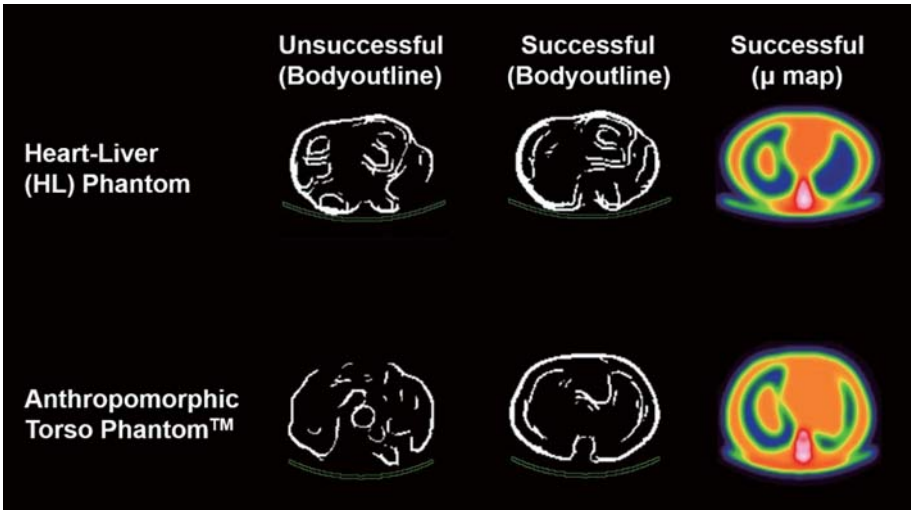

Fig. 5 Single photon emission computed tomography (SPECT) image of two different myocardial phantoms. The left images have unsuccessful body outline extraction, the center images have successful body outline extraction, and the right images have a successful μ map.

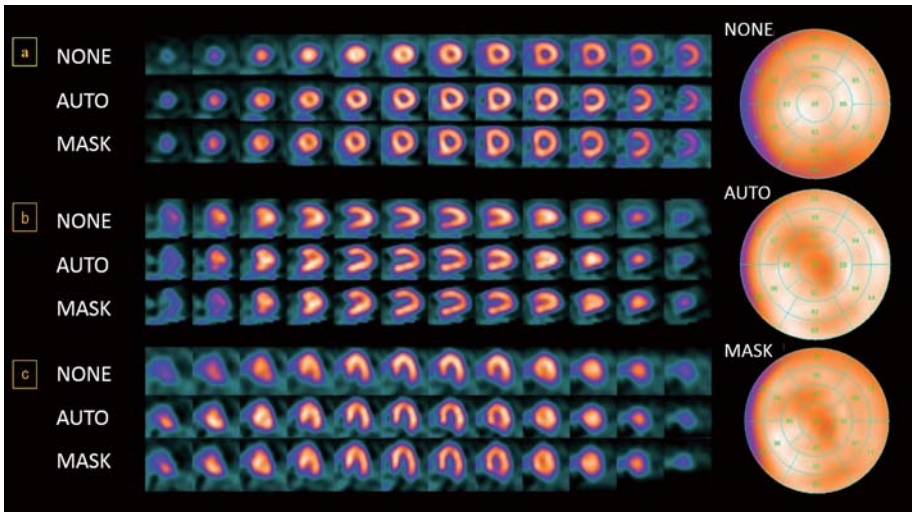

Fig. 6 SPECT images of normal case: comparison of NONE (top), AUTO (middle), and MASK (bottom) stress short axis (a), horizontal (b) and vertical long-axis (c) myocardial perfusion images and polar maps.

count leading to truncations in the body outline. However, the success rate was improved to 99% by using the masking process. The success rate of SSPAC in the resting condition was 100% by automatic processing only. In the NONE, AUTO and MASK groups, RCA, LAD and LCX showed equal contrast values. In the RCA, LAD and LCX groups, NONE, AUTO and MASK showed equal contrast values (Fig. 3, 4). There were significant differences between before and after SSPAC correction ($p<0.05$).

Fig. 6 shows SPECT images of a normal subject: a 69-year old male without coronary artery disease. The uncorrected myocardial perfusion images reveal an apparent perfusion abnormality in the basal inferior wall. However, after attenuation correction with the AUTO method, a more uniform tracer distribution is apparent.

Fig. 7 shows SPECT images of ischemic heart disease of the LAD in a 62-year-old female with significant stenosis of the diagonal branch of the LAD coronary artery. The uncorrected myocardial perfusion images reveal a perfusion abnormality in the anterior wall. After the AUTO method, the perfusion abnormality is clearly apparent in the anterior wall.

Discussion

Scatter-, attenuation- and spatial-resolution corrections are required for SPECT in order to improve the accuracy of quantification (9). The dual-energy window subtraction (DEWS) method (10), the effective scatter source estimation (ESSE) method (11), and the TEW method (6) are used for scatter correction. The Chang method (12), the external source method (1), and the X-ray CT method (2) are used for attenuation correction. The Frequency-Distance Relationship

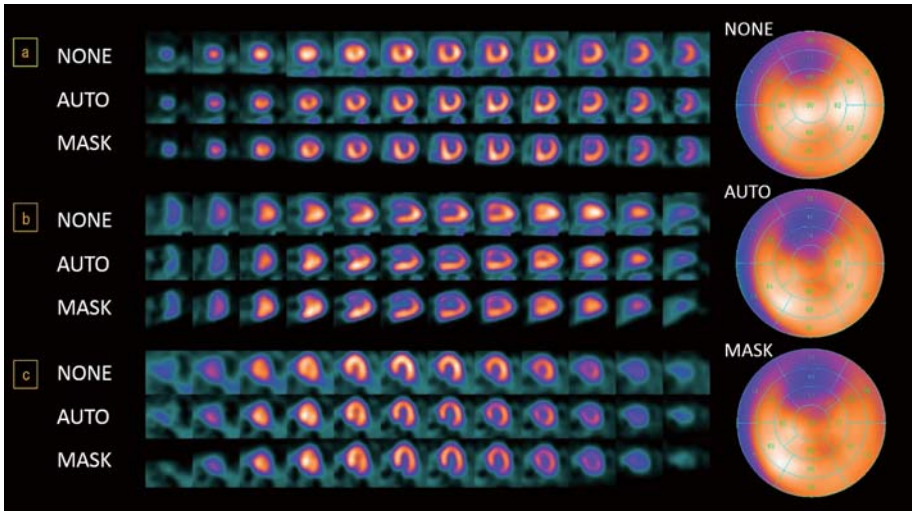

Fig. 7 SPECT images of ischemic heart disease of the LAD: comparison of NONE (top), AUTO (middle), and MASK (bottom) stress short axis (a), horizontal (b) and vertical long-axis (c) myocardial perfusion images and polar maps.

(FDR) method (13) and the collimator board correction (CBC) method (14) are used in spatial resolution correction. These correction methods have recently been incorporated into an iterative algorithm (15). In addition, it has recently been argued that a correction for the partial volume effect (16) is also necessary. Each correction method has merits and demerits.

We performed attenuation correction by using CT images (CTAC). CTAC has several advantages, such as improving the accuracy of the μ map and shortening the acquisition time. However, the radiation dose exposure from CT must be considered. Simultaneous Compton Scatter is performed during SPECT acquisition. This method use different μ levels to the lungs, mediastinum, heart, and bone and can be used practically after the body outline extraction. Additional acquisition time is not needed and the agreement is superior between SPECT image and μ levels by using this method. This method also reduces the mental and physical stresses on the patient.

CTAC is performed with a free breathing or breath-hold in myocardial SPECT. However, the positions of the heart, lungs and diaphragm scanned by CT image in short time are not same as those evaluated by the myocardial SPECT in the free breathing. Therefore, the artifacts on CTAC may be caused by misregistration of CT and SPECT, and this problem is also not settled in hybrid SPECT/CT equipment (17). On the other hand, this problem is conquered by SSPAC. It has been reported that SSPAC provides more uniform distribution of myocardial perfusion than CTAC (18,19).

In contrast, decreases in apical and apex activities were observed between NONE and AUTO, MASK in normal case (Fig. 6). These decreases are a well-known phenomenon in attenuation corrected myocardial perfusion (20, 21). "Apical thinning" on the SSPAC image may be caused by both low attenuation corrected myocardial uptake and myocardial thinning.

SSPAC method is useful, but its use has not become widespread due to failure in extraction of the body outline and thus inaccurate segmentation. The cause of this is a low rotation count leading to truncated imaging of the outline. SSPAC alone cannot distinguish the body outline and the lung contour in these conditions.

Yamauchi et al.(4) reported that the automatic processing success rate of SSPAC was 93%. They used low counts, and SSPAC was not successful in the stress condition, but a μ map made in a resting-condition study with a high count can be used under stress. Elsewhere, the success rate of SSPAC with 201TlCl was reported to be 73% (5).

The mask processing of the lung contour increased success rate from 44% to 99%. Because clinical studies require high success rates, we anticipate that the use of this mask processing method will lead to more widespread use of SSPAC.

Conclusion

Generation of the map in the SSPAC method is affected by the low count (stress condition) in myocardial SPECT. Our method for masking will contribute to a widespread use of SSPAC by improving the success rate in contouring.

Acknowledgments

This work was partly supported by Department of Radiology, Gunma University Hospital and Mr. Kazumasa Fujioka of Toshiba Medical Systems Corporation.

Sources of funding

None

Conflicts of interest

The authors declare that they have no conflict of interest.

Reprint requests and correspondence:
Takao Kanzaki, MS
Department of Radiology, Gunma University Hospital, 3-19-15 Showa, Maebashi, Gunma, Japan 371-8511
E-mail: tkanzaki@gunma-u.ac.jp

References

1. Murase K, Tanada S, Inoue T, et al. Improvement of brain single photon emission tomography (SPET) using transmission data acqusition in a four-head SPET scanner. Eur J Nucl Med 1993; 20: 32-8.
2. Patton JA, Delbeke D, Sandler MP. Image fusion using an integrated, dual-Head coincidence camera with X-ray tube-based attenuation maps. J Nucl Med 2000; 41: 1364-8.
3. Murase K, Tanada S, Inoue T, et al. Effect of misalignment between transmission and emission scans on SPECT images. J Nucl Med Technol 1993; 21: 152-6.
4. Yamauchi Y, Kanzaki Y, Otsuka K, et al. Novel attenuation correction of SPECT images using scatter photopeak window data for the detection of coronary disease. J Nucl Cardiol 2014; 21: 109-17.
5. Sasaki T, Tsunoda T, Kato R, et al. Evaluation of SSPAC method in the ^{201}TlCl myocardial scintigraphy. J Nayoro City Hospital 2011; 19: 24-6. (in Japanese)
6. Ogawa K. Simulation study of triple-energy-window scatter correction in combined Tl-201, Tc-99m SPECT. Ann Nucl Med 1994; 8: 277-81.
7. Hudson HM, Larkin RS. Accelerated image reconstruction using ordered subsets of projection data. IEEE Trans Med Imaging 1994; MI-13: 601-9.
8. Takahashi Y, Murase K, Mochizuki T, et al. Evaluation of the number of SPECT projections in the ordered subsets-expectation maximization image reconstruction method. Ann Nucl Med 2003; 17: 525-30.
9. Takahashi Y. Data acquisition and image processing related to changes in nuclear cardiology devices. Ann Nucl Cardiol 2015; 1 (1): 132-135.
10. Jaszczak RJ, Greer KL, Floyd CE Jr, et al. Improved SPECT quantification using compensation for scattered photons. J Nucl Med 1984; 25: 893-900.
11. Frey EC, Tsui BMW. A new method for modeling the spatially-variant, object-dependent scatter response, function in SPECT. IEEE Nucl Sci Symp 1996; 2: 1082-6.
12. Chang LT. A method for attenuation correction in radionuclide computed tmography, IEEE Trans Nucl Sci 1978; NS-25, 638-43.
13. Edholm PR, Lewitt RM, Lindholm B. Novel properties of the Fourier decomposition of the sonogram. Proc. SPIE1986; 671: 8-18.
14. Takahashi Y, Murase K, Mochizuki T, et al. Simultaneous three-dimensional resolution correction in SPECT reconstruction using OS-EM algorithm. J Nucl Med Tech 2007; 35: 34-8.
15. El Fakhri G, Buvat I, Benali H, et al. Relative impact of scatter, collimator response, attenuation, and finite spatial resolution corrections in cardiac SPECT. J Nucl Med 2000; 41: 1400-8.
16. Hutton BF, Osiecki A. Correction of partial volume effects in myocardial SPECT. J Nucl Cardiol 1998 5: 402-13.
17. McQuaid SJ, Hutton BF. Sources of attenuation-correction artefacts in cardiac PET/CT and SPECT/CT. Eur J Nucl Med Mol Imaging 2008; 35: 1117-23.
18. Hiroyuki F. Reduction of the attenuation artifact in SSPAC in Myocardial SPECT, INNERVISION; 2011; 4: 40-1 (in Japanese).
19. Hisato M, Sei S, Satoshi H, et al. Attenuation Correction in Myocardial SPECT Imaging − Generation of Estimated Patient-Specific Attenuation Maps From Scatter and Photopeak Window Data, Toshiba medical review; 2003; 91 (in Japanese).
20. Okuda K, Nakajima K, Matsuo S, et al. Cause of apical thinning on attenuation-corrected myocardial perfusion SPECT. Nucl Med Commun 2011; 32: 1033-9.
21. Links JM, Becker LC, Anstett F. Clinical significance of apical thinning after attenuation correction. J Nucl Cardiol 2004; 11: 26-31.